Citation: CPT Pharmacometrics Syst. Pharmacol. (2015) 4, 286–294; doi:10.1002/psp4.35

ORIGINAL ARTICLE

Integration of Physiologically-Based Pharmacokinetic Modeling into Early Clinical Development: An Investigation of the Pharmacokinetic Nonlinearity

L Zhou[1], J Gan[1], H Yoshitsugu[2,3], X Gu[1], JD Lutz[1], E Masson[2,4] and WG Humphreys[1]

BMS-911543, a promising anticancer agent, exhibited time-dependent and dose-dependent nonlinear pharmacokinetics (PKs) in its first-in-human (FIH) study. Initial physiologically based pharmacokinetic (PBPK) modeling efforts using CYP1A2-mediated clearance kinetics were unsuccessful; however, further model analysis revealed that CYP1A2 time-dependent inhibition (TDI) and perhaps other factors could be keys to the nonlinearity. Subsequent experiments in human liver microsomes showed that the compound was a time-dependent inhibitor of CYP1A2 and were used to determine the enzyme inactivation parameter values. In addition, a rat tissue distribution study was conducted and human plasma samples were profiled to support the refinement of the PBPK model. It was concluded that the interplay between four BMS-911543 properties, namely, low solubility, saturation of the metabolizing enzyme CYP1A2, CYP1A2 TDI, and CYP1A2 induction likely resulted in the time-dependent and dose-dependent nonlinear PKs. The methodology of PBPK model-guided unmasking of compound properties can serve as a general practice for mechanistic understanding of a new compound's disposition.
CPT Pharmacometrics Syst. Pharmacol. (2015) **4**, 286–294; doi:10.1002/psp4.35; published online on 29 April 2015.

Study Highlights

WHAT IS THE CURRENT KNOWLEDGE ON THE TOPIC? ☑ Very few studies have been published on PBPK models that quantitatively address clinical PK questions for a compound in early clinical development. Even fewer have described the process of forward and back translation between model and *in vitro* experimentation. • WHAT QUESTION DID THIS STUDY ADDRESS? ☑ The PBPK model described in this study characterized the mechanism of the dose-dependent and time-dependent PK nonlinearity of BMS-911543. It also addressed the general question of how PBPK modeling in the early development of a new drug can facilitate the overall understanding of drug disposition • WHAT THIS STUDY ADDS TO OUR KNOWLEDGE ☑ The study demonstrated that a plausible PBPK model can be constructed for a compound with complex ADME properties, even like BMS-911543, to address its nonlinear PKs arising in early clinical development, but will likely require researchers to use a forward and back translation paradigm between experimentation and model. HOW THIS MIGHT CHANGE CLINICAL PHARMACOLOGY AND THERAPEUTICS ☑ The PBPK model-guided approach of reverse translation of ADME information is particularly useful in selectively challenging early assumptions followed by conducting nonclinical studies in order to rapidly improve the predictability of early PBPK models.

Current strategies in drug discovery are capable of producing new drug candidates with acceptable nonclinical absorption, distribution, metabolism, and excretion (ADME) properties.[1] However, translation of that ADME information, which is obtained either from *in vitro* systems or from animal species, into understanding of the behavior of the new drug in humans is not always straightforward. For instance, a drug candidate may exhibit an unexpected dose-dependent and time-dependent pharmacokinetic (PK) behavior in first-in-human (FIH) studies. Often, the underlying ADME properties linked to the unfavorable dose-dependent and time-dependent PKs are difficult to identify because of the highly convoluted nature of the clinical PK parameters. Lack of knowledge of the underlying ADME liability makes it difficult to mitigate such clinical PK issues during drug development.

Utilization of physiologically based pharmacokinetic (PBPK) modeling to provide an integrated analysis of complex PK phenomena has been recognized for some years.[2] By constructing quantitative relationships among demographic, physiological, genomic, and ADME properties, a PBPK model can provide mechanistic understanding as well as diagnostic and predictive value. The explosive increase in computing power in the past decades has enabled PBPK modeling platform development and the field has steadily matured and has seen broader utilization. Pharmaceutical companies have become increasingly dependent on PBPK models to provide decision-making analysis of PK-driven questions.[3] Additionally, a limited number of regulatory decisions have been made based on PBPK modeling to address clinical pharmacology questions.[4] Whereas a plausible PBPK model can frequently be developed for drug candidates at an advanced stage of clinical development in which ADME properties have been well characterized, major challenges exist when developing PBPK models for compounds

[1]Department of Biotransformation, Bristol-Myers Squibb, Princeton, New Jersey, USA; [2]Exploratory Clinical and Translational Research, Bristol-Myers Squibb, Princeton, New Jersey, USA; [3]Current affiliation: Clinical Pharmacology & PPDM, Japan Development, MSD K.K., Tokyo, Japan; [4]Current affiliation: Quantitative Clinical Pharmacology, AstraZeneca, Waltham, Massachusetts, USA. Correspondence: L Zhou (lianunc@gmail.com)
Received 10 December 2014; accepted 20 March 2015; published online on 29 April 2015. doi:10.1002/psp4.35

in early clinical investigation.[5] Challenges for early development of PBPK models usually arise because of insufficient ADME information, which leads to the incorporation of multiple assumptions and calculated parameters. In addition, there are often difficulties in the translation of preclinical ADME data into clinical predictions.

BMS-911543 (see **Supplementary Figure S1** for structure), a highly selective Janus Kinase 2 inhibitor, exhibited favorable efficacy and safety as well as ADME properties *in vitro* and in animals (**Supplementary Table S1**) and was thus advanced into clinical development for treatment of myeloproliferative neoplasms.[6] The permeability of BMS-911543 across caco-2 monolayers was high with a permeability coefficient (5×10^{-5} cm/s for BMS-911543; 2.5×10^{-5} cm/s for metoprolol; 1.2×10^{-5} cm/s for verapamil) comparable to the values for compounds that exhibit good absorption in humans.[7] Studies in bile-duct cannulated rats revealed that the direct excretion of BMS-911543 in bile and urine was minimal, accounting for $<2\%$ of total clearance. The primary metabolic elimination found for BMS-911543 in liver microsomes and in bile-duct cannulated rats was mainly attributed to the metabolism by cytochrome P450 (CYP) 1A2, which mediated the formation of metabolite M1 (see **Supplementary Figure S1** for structure). Metabolite M1 was the only major metabolite identified *in vitro* and in animals. The half maximal inhibitory concentration value of BMS-911543 in incubations with tacrine as the CYP1A2 activity probe did show a modest level of interaction with the enzyme, however, detailed study of enzyme kinetics or the potential for CYP1A2 time-dependent inhibition was not explored before clinical studies. Unexpectedly, BMS-911543 exhibited a dose-dependent and time-dependent PK nonlinearity in the FIH study conducted in patients with cancer.[8]

To investigate the mechanism of dose-dependent and time-dependent PK nonlinearity for BMS-911543, a PBPK modeling methodology was applied, which enabled the bidirectional translation (forward and reverse translation) of the compound's ADME information. The forward translation used the available nonclinical ADME data to predict the PK behaviors of BMS-911543. The reverse translation utilized the discrepancies between predicted and observed PK behaviors in order to determine which nonclinical studies should be conducted. The PBPK model then evolved by addition of the newly generated nonclinical data, and this optimized model was used to propose the mechanism of the dose-dependent and time-dependent PK nonlinearity. The methodology of model-guided bidirectional translation of ADME information can serve as a general practice for mechanistic understanding of a new drug's PKs during its early clinical development.

METHODS

BMS-911543 metabolism

Kinetics of M1 formation was determined after incubation of BMS-911543 (0.1–10 μM) with recombinant CYP1A2, CYP3A4, CYP2J2, and human liver microsomes (HLMs; 0.25 mg/mL) supplemented with 1 mM reduced nicotinamide adenine dinucleotide phosphate in pH 7.4 phosphate buffer at 37 °C for 10 minutes. The reaction was terminated by the addition of an equal volume of acetonitrile, and the resulting supernatant was analyzed by LC/MS/MS. All experiments were performed in triplicate. The Michaelis-Menten constant (K_m) and the maximum rate of metabolite formation (V_{max}) were determined by nonlinear fitting using GraphPad Prism (La Jolla, CA) and are presented as mean and SE.

CYP1A2 time-dependent inhibition

Acetaminophen formation from phenacetin was monitored as the CYP1A2 activity probe reaction. BMS-911543 (0, 0.39, 0.78, 1.56, 3.125, 6.25, 12.5, and 25.0 μM) was preincubated with 1.0 mg/mL HLMs in 100 mM potassium phosphate buffer at pH 7.4 and 37 °C. After a 5-minute preincubation, time-dependent inhibition (TDI) was initiated with the addition of 1 m*M* final concentration of nicotinamide adenine dinucleotide phosphate and allowed to incubate for 3, 10, 20, and 30 minutes in the absence of phenacetin. Aliquots of the incubation mixture were then diluted 10-fold into wells containing 1 m*M* nicotinamide adenine dinucleotide phosphate and phenacetin (450 μM final concentration) and allowed to incubate for 13.5 minutes. After reaction quenching, the resulting supernatants were injected into LC/MS/MS for analysis.

The TDI parameters associated with half maximum rate of inactivation (K_I) and the maximum rate of enzyme inactivation (k_{inact}) were determined by the following equations:

$$v_I = v_0 e^{-\lambda t} \quad (1)$$

where λ is:

$$\lambda = \frac{k_{inact} I}{K_I + I} \quad (2)$$

t, v_I and v_0 are time and reaction velocity at a specific initial inhibitor concentration (I) or no inhibitor control, respectively. Velocity data was transformed to percent of maximum velocity (no inhibitor control). Inhibition constants were determined via nonlinear regression using GraphPad Prism v.5 and are presented as mean and SE.

FIH study design and plasma sample collection

PKs of BMS-911543 was determined in an open label, multiple dose escalation (5, 10, 20, 40, 80, 120, 160, 200, and 240 mg) study of patients with cancer. Patients included 52 men and women aged 18 and over from 5 international locations. The study consisted of a single-dose period and a multiple-dose period, with a total dosing period of 15 days. In the single-dose period (day 1), a single dose of BMS-911543 was administered, followed by a 24-hour washout period. BMS-911543 was then administered continuously twice-daily (b.i.d.) for two weeks in the multiple-dose period. Plasma samples were collected at 0.5, 1.0, 2.0, 3.0, 4.0, 6.0, 8.0, 12.0, and 24.0 hours post-dose on day 1 and at 0, 0.5, 1.0, 2.0, 3.0, 4.0, 6.0, 8.0, and/or 12.0 hours post-dose on day 15 from 72 subjects with a total of 833 timepoints. Study protocol and patient informed consents were approved by an institutional review board at each study center. The study was conducted in accordance

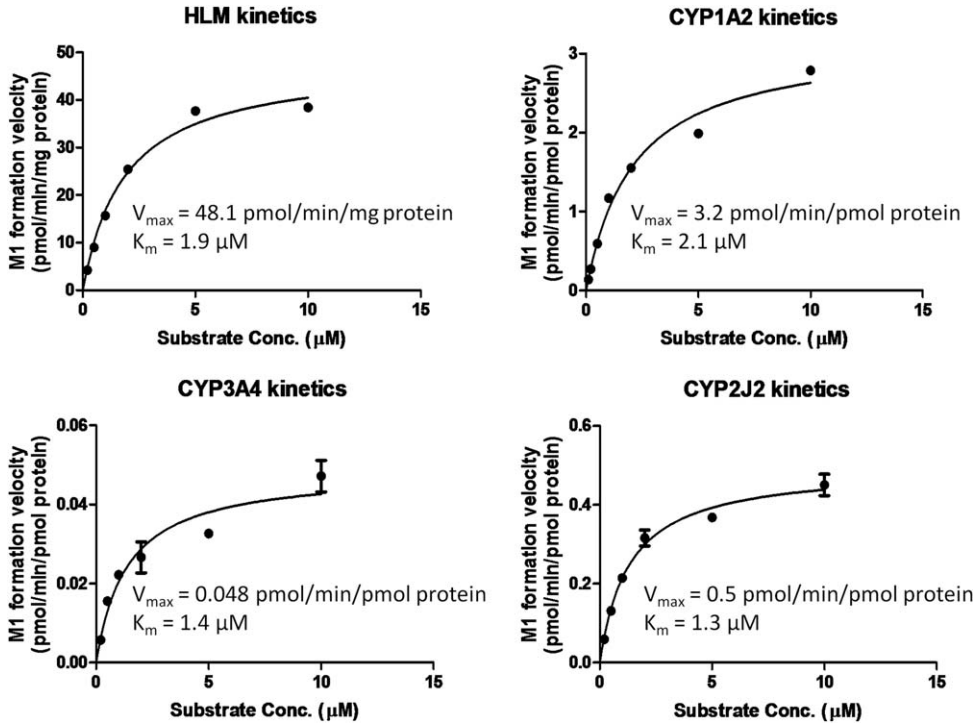

Figure 1 The formation rate profiles of metabolite M1 after incubation of BMS-911543 in pooled human liver microsomes (HLMs) and in recombinant CYP1A2, CYP3A4, and CYP2J2. Values are the mean of three measurements ± SD.

with the principles of the Declaration of Helsinki and Good Clinical Practice. The clintrial.gov number for BMS-911543 is NCT01236352.

PBPK modeling and simulation

A PBPK model was constructed for BMS-911543 using a population-based ADME simulator (V12; SimCYP, Sheffield, UK). The compound-related parameters used to build the PBPK model for BMS-911543 are based on ADME properties available before this study and the results described in this article (**Supplementary Tables S1 and S3**).

The total clearance of BMS-911543 was primarily defined by the metabolic clearance. The metabolic clearance was defined by enzyme kinetic parameters. V_{max} and K_m values were determined from the formation rate of metabolite M1 in CYP1A2, CYP3A4, and CYP2J2 recombinant systems (**Figure 1**). The fu_{mic}, the unbound fraction of the BMS-911543 in incubation with 0.25 mg/mL microsomal protein, was predicted to be 0.78 using the built-in method. A metabolic scaling factor of 4 was applied to the parameters of K_m (input as K_m/4) for CYP1A2, CYP3A4, and CYP2J2 to recover the discrepancy observed from *in vitro* to *in vivo* extrapolation. The value of scaling factor was obtained by the best fitting to the FIH day 1 plasma concentration data.

The magnitude of BMS-911543 accumulation after multiple dosing was mainly defined by CYP1A2 TDI and induction parameters. The parameters describing the potency of CYP1A2 TDI and induction were determined from *in vitro* experiments. The input for CYP1A2 K_I (11.2 μM) was allowed to deviate from the experimental value (2.9 μM) to achieve the best fitting to the clinical data. The values for other parameters (the maximal fold induction over vehicle E_{max}, inducer concentration that supports half maximal induction EC_{50}, and TDI inactivation parameter k_{inact}) were input as the experimental values.

The plasma concentration-time profiles of BMS-911543 in humans were simulated at 5, 10, 20, 40, 80, 120, 160, 200, and 240 mg, according to the dosing regimens set in the clinical protocol. Simulation was performed in 10 trials, with 10 subjects in each trial, which led to a total of 100 simulations per dose. A healthy volunteer population was used for the demographics data, as provided in the software. All other demographic, physiological, and genomic parameters were used as the default values.

RESULTS

BMS-911543 metabolism

The formation rate profiles of M1 after incubation of BMS-911543 (0.1–10 μM) in recombinant CYP1A2, CYP3A4, CYP2J2, and pooled HLM are shown in **Figure 1**. Preliminary studies had shown that these three enzymes were the only CYP enzymes capable of producing M1 (data not shown). The observed enzyme kinetic values for V_{max} and K_m are listed in **Figure 1**. Metabolite M1 was the only drug-related component detected in cDNA-expressed CYP enzymes and pooled HLMs, indicating that the formation of this metabolite is the primary biotransformation pathway for BMS-911543. All three CYP enzymes, CYP1A2, CYP3A4, and CYP2J2, were found to mediate the formation of M1 (**Figure 1**). The kinetic data, along with the CYP inhibition study using HLMs in the presence of specific CYP inhibitors

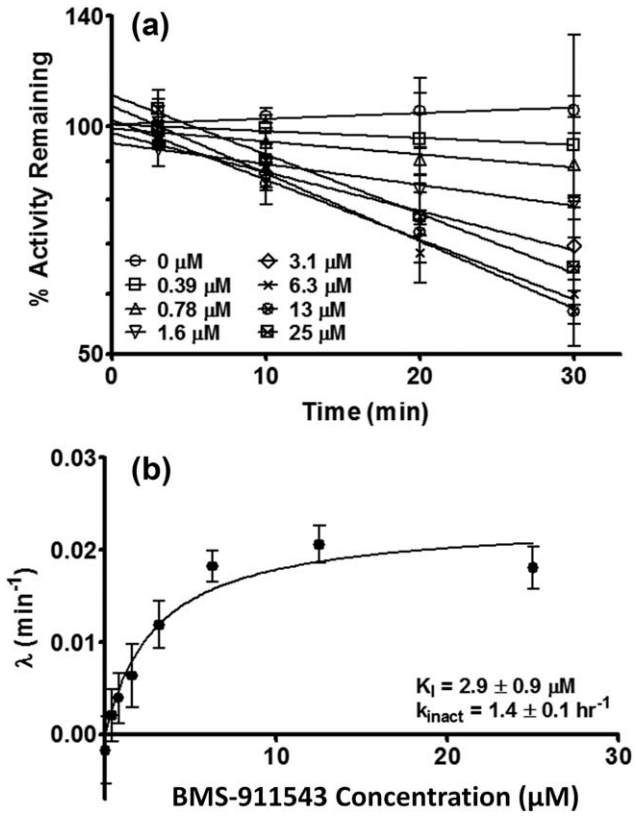

Figure 2 The time-dependent inhibitory effect of BMS-911543 on CYP1A2 in human liver microsomes. (**a**) A plot of the log percent CYP1A2 activity remaining vs. incubation time. (**b**) A plot of the initial rate constant of inactivation (λ) vs. the initial inhibitor concentration (I). Values are the mean of three measurements ± SD.

(data not shown), indicated that CYP1A2 was the primary enzyme mediating the formation of M1 and also suggested that CYP3A4 and CYP2J2 played a minor role.

CYP1A2 TDI by BMS-911543

The TDI effect of BMS-911543 on acetaminophen formation from phenacetin in HLMs is shown in **Figure 2**. The initial rate constant for enzyme inactivation (the slope, λ) at each concentration of BMS-911543 (0, 0.39, 0.78, 1.56, 3.125, 6.25, 12.5, and 25.0 μM) is shown in **Figure 2a**. The determination of the TDI parameters (K_I and k_{inact}) is depicted in **Figure 2b**. The values of K_I and k_{inact} were determined to be 2.9 ± 0.9 μM and 1.4 ± 0.1 h^{-1}, respectively.

Pharmacokinetics of BMS-911543

Figure 3 shows the plasma concentration vs. time profiles for BMS-911543 after single and multiple administration of BMS-911543 to patients with cancer. BMS-911543 was absorbed rapidly after oral administration. After absorption was completed, the plasma concentration of BMS-911543 decreased quickly. The values of $t_{1/2}$ were smaller than 3 hours at 5–40 mg doses (2.0, 1.9, 2.8, and 2.8 hours at doses of 5, 10, 20, and 40 mg, respectively). However, at doses higher than 40 mg, $t_{1/2}$ values were prolonged. The values of $t_{1/2}$ were 3.2, 2.7, 5.7, 4.0, and 4.9 hours at doses of 80, 120, 160, 200, and 240 mg, respectively. BMS-911543 did not accumulate in plasma after two-week multiple dosing at doses of 5, 10, and 20 mg. Accumulation was observed at doses of 40 mg b.i.d. and higher and increased with increase of dosage. **Figure 4** depicts observed dose-dependence of peak plasma concentration (C_{max}) and area under the curve (AUC) after single (solid dots in **Figure 4a** and **4b**) and multiple (solid dots in **Figure 4c** and **4d**) dosing of BMS-911543. The exposure (C_{max} and AUC) of BMS-911543 was presented as an approximately dose-proportional increase on day 1. Consistent with the accumulation observed after multiple dosing ($\geq$40 mg), the values of C_{max} and AUC increased in a greater than dose proportional manner after multiple dosing at doses higher than 40 mg. These results suggested dose-dependent and time-dependent change of CL/F. Volume of distribution at steady state (V_{ss})/F could not be calculated because of insufficient data after repeated dosing. However, preliminary population PK analysis suggested that V_{ss}/F was about 50 L.

PBPK modeling and simulation

The initial modeling attempts were based on BMS-911543 ADME properties available before this study and the elimination enzyme kinetics described in this article (**Supplementary Table S1**). The initial models overpredicted the day 1 plasma concentration-time profiles in general, and failed to describe the accumulation of BMS-911543 concentrations in plasma after multiple dosing (data not shown).

The fully optimized model was constructed after the incorporation of the nonclinical parameters described in this article. **Figure 2** shows the predicted dose-dependence of C_{max} and AUC after single (open squares in **Figure 4a** and **4b**) and multiple (open squares **Figure 4c** and **4d**) dosing of BMS-911543. The predicted dose-dependent changes of C_{max} and AUC were consistent with the observed data. The observed concentration-time profiles for all doses were well contained within the simulated 5th and 95th percentiles (data not shown). A representation of observed vs. predicted plasma concentrations-time profiles of BMS-911543 is shown in **Figure 5** (see **Supplementary Table S2** for observed plasma concentrations). The model predicted the absorption rate constant (k_a) to be 4.138 h^{-1}. The fraction of dose absorbed (F_a) was predicted to be dose-dependent and would decrease from 1 to 0.42 over the dose range of 5–240 mg, suggesting the absorption of BMS-911543 is a saturable process.

The predicted fraction of drug escaping the gut wall metabolism (F_g) was unity, suggesting metabolic enzymes in the gut were not involved in the elimination of BMS-911543. The predicted fraction of metabolism by CYP1A2 was 96% of the total clearance, indicating CYP1A2 was the dominant enzyme responsible for the elimination of BMS-911543. Multiplying the day 1 apparent clearance ($dose/AUC_{day\ 1}$) by F_a to negate the effect of changes in absorption, the adjusted apparent clearance ($CL_{adjusted} = F_a \times dose/AUC_{day\ 1}$) decreased from 11.3 to 7.3 L/h over the dose range. Because F_g was unchanged, $CL_{adjusted}$ reflects hepatic metabolism only. The values of $CL_{adjusted}$

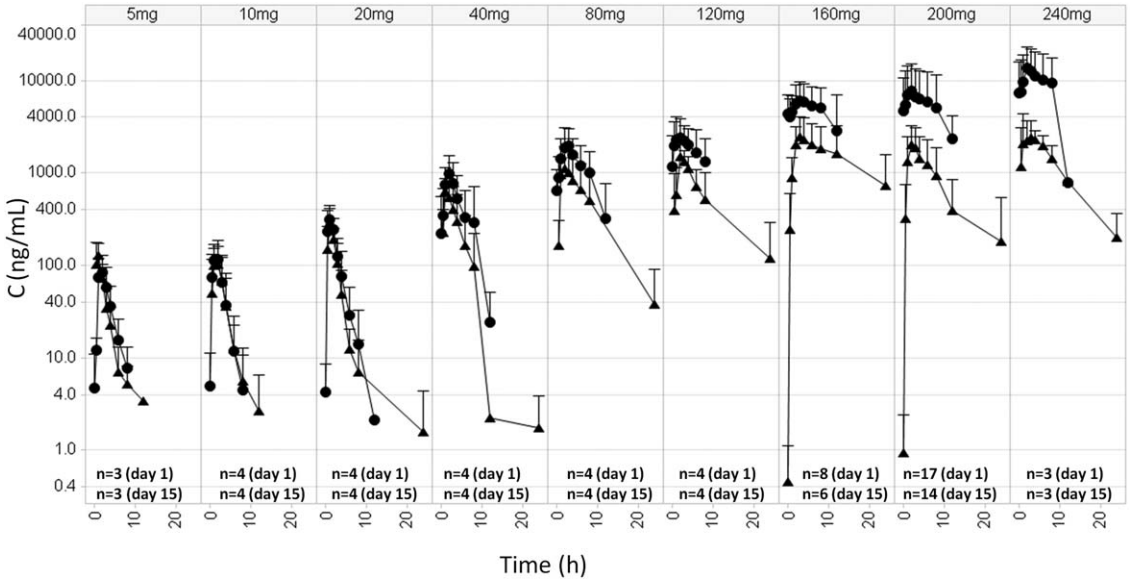

Figure 3 The mean plasma concentration-time profiles of BMS-911543. Day 1 data is indicated by filled triangles. Day 15 data is represented by filled circles. Values are mean ± SD. The patient number is indicated by "n."

decreased suggesting saturation of hepatic metabolism (e.g., CYP1A2) occurred. Dose-dependent decrease of $CL_{adjusted}$ after single dosing of BMS-911543 is shown in **Figure 6a**. The effect on CYP1A2 activity by time-dependent inhibition and induction in the liver over 15-day dosing of 200 mg BMS-911543 is depicted in **Figure 6b**.

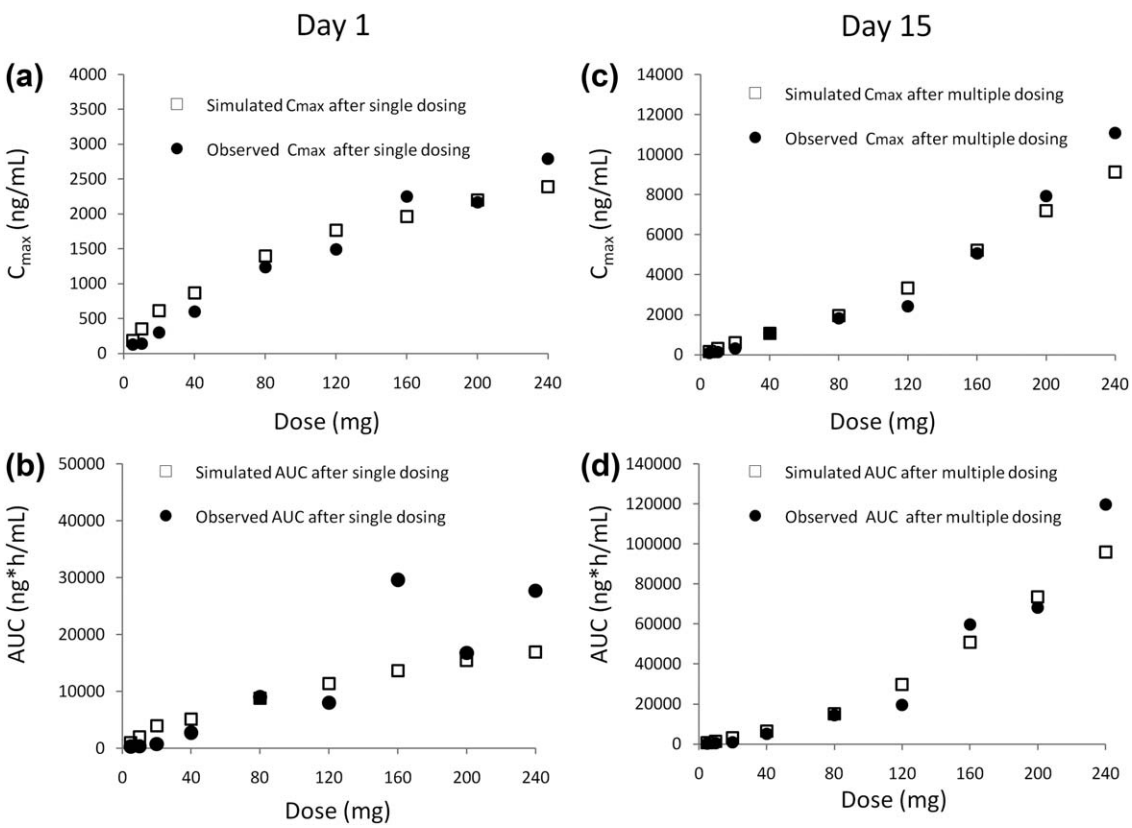

Figure 4 Observed vs. predicted dose-dependence of peak plasma concentration (C_{max}) and area under the curve (AUC) after single (**a and b**) and multiple (**c and d**) dosing of BMS-911543. AUC values reported are mean AUC(INF) for day 1 and mean AUC(0–12 h) for day 15.

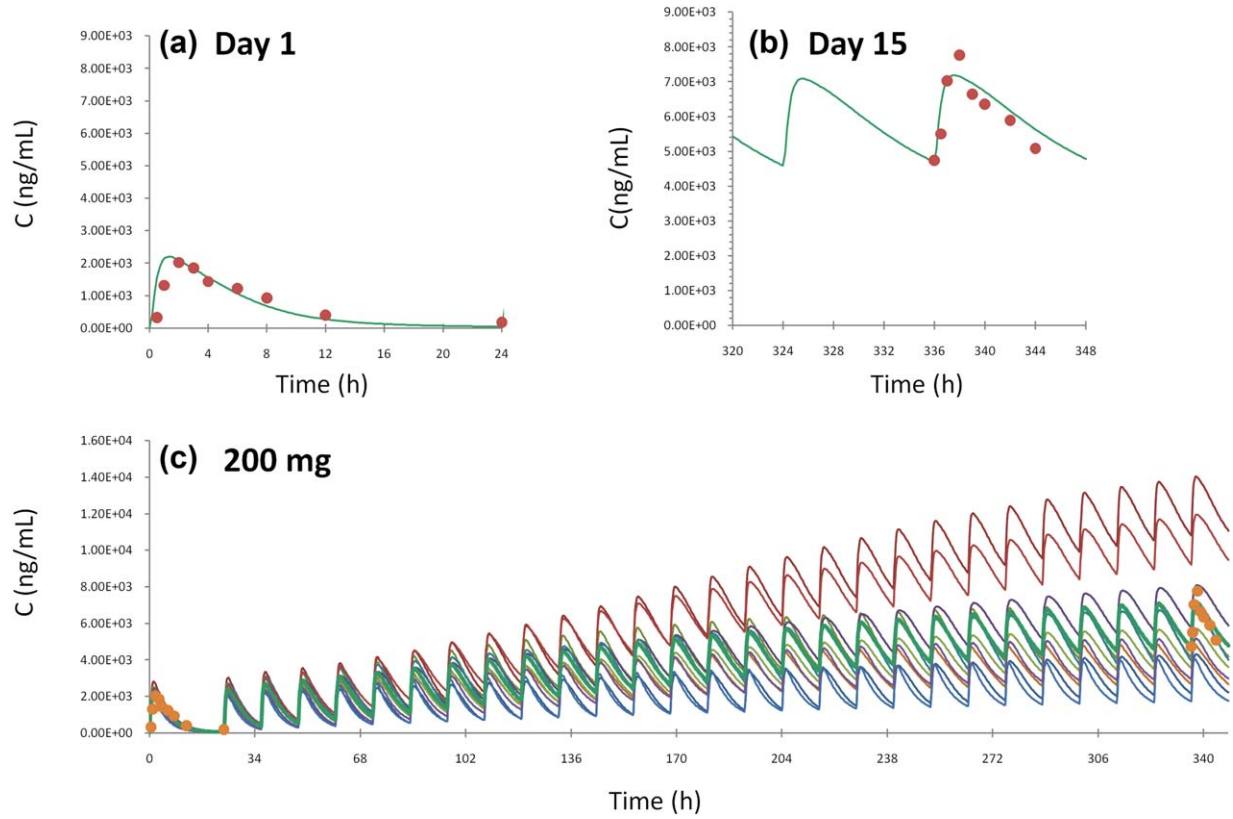

Figure 5 A representation of the observed vs. predicted concentration-time profiles of BMS-911543 for 15 days at 200 mg dosing. (**a**) The day 1 predicted mean concentration-time profile (line) and observed data (dots). (**b**) The day 15 predicted mean concentration-time profile (line) and observed data (dots). (**c**) The concentration-time profiles of BMS-911543 over 15-day dosing. The thin lines represent individual trials and the thick line is the mean of the 10 trials. Mean observed data is indicated by solid dots.

The CYP1A2 activity was reduced gradually over the course of dosing. By day 15, there was ~62% of the CYP1A2 activity remaining in the liver in the presence of impact by both TDI and induction (grey line, **Figure 6b**). Because CYP1A2 induction will attenuate TDI, simulations were performed in the absence of induction to determine the magnitude of attenuation by induction. The percentage of CYP1A2 activity remaining dropped to 54% by day 15 in

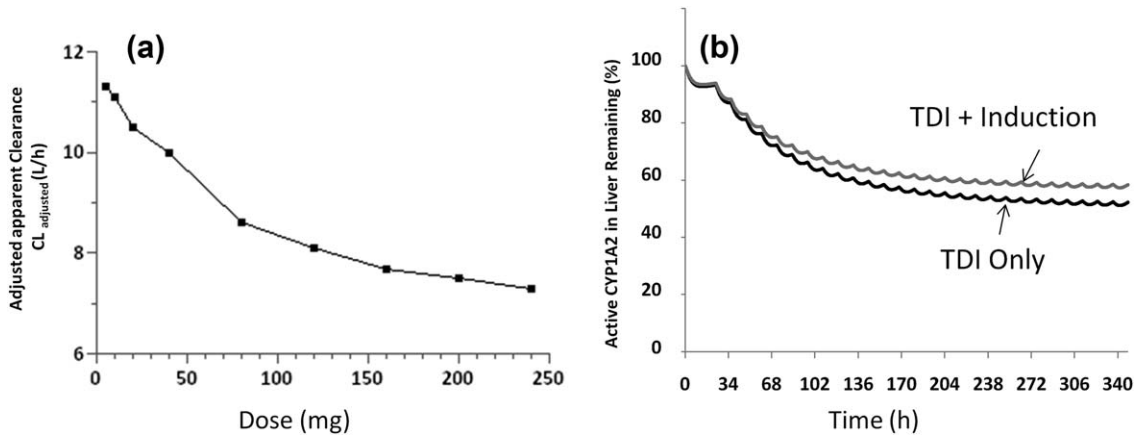

Figure 6 Effect of saturation of metabolism on clearance of BMS-911543 (**a**) and the impact of time-dependent inhibition (TDI) and autoinduction of CYP1A2 on active CYP1A2 level (**b**) simulated by the physiologically based pharmacokinetic (PBPK) model. (**a**) Dose-dependent decrease of adjusted apparent clearance ($CL_{adjusted}$) after single dosing of BMS-911543 (day 1) reflected saturation of metabolism. $CL_{adjusted}$ is a product of multiplying the apparent clearance ($dose/AUC_{day\ 1}$) by F_a to negate the effect of changes in absorption. (**b**) The decrease of active CYP1A2 enzyme level in liver reflected time-dependent changes in BMS-911543 metabolism over 15-day dosing of BMS-911543.

the absence of induction (black line, **Figure 6**b), indicating that TDI alone produced a 46% reduction of the CYP1A2 activity. The difference in CYP1A2 activity remaining in the presence or absence of induction was 8%, suggesting that the magnitude of attenuation on TDI by induction was 17% (8% of 46%).

DISCUSSION

Modeling of compounds in early clinical development is challenging because of a lack of understanding of many aspects of the compound's PK/ADME behavior. For BMS-911543, the early modeling efforts demonstrated that there were gaps in our understanding leading to a poor description of the nonlinear PK behavior and that we needed to refine our dataset, especially around the enzymatic clearance of the compound.

The final PBPK model suggested that the dose-dependent and time-dependent nonlinearity of BMS-911543 exposure is driven by the interplay between four ADME properties of the compound: (1) the low solubility of the compound limits its absorption at high doses; (2) saturation of metabolism contributes to the nonlinearity by producing a decrease in hepatic clearance (from 11.3–7.3 L/h) over the dose range; (3) CYP1A2 TDI is the key factor leading to the time-dependent PK nonlinearity; (4) CYP1A2 auto-induction produces attenuation of TDI. BMS-911543 produced an approximately dose-proportional increase in exposure on day 1 because of the following two reasons. First, solubility-limited absorption apparently eliminated the effect of saturation of metabolism on day 1. Second, the effect of both CYP1A2 TDI and induction is limited because each effect is time-dependent and would be expected to take longer than 1 day to produce significant impact on BMS-911543's exposure. On day 15 after two weeks of dosing, the impact of TDI and induction are likely to be fully exhibited, which manifests as a dose-dependent increase in exposure because of the predominant effect of TDI.

The PBPK model was utilized to tease out the impact of solubility and permeability on the absorption of BMS-911543. Sensitivity analysis of the impact on absorption by the solubility and permeability parameters revealed that BMS-911543 absorption was dose-dependent (**Supplementary Figure S3**). The finding that F_a is not sensitive to the changes of permeability (**Supplementary Figure S3A**) is in agreement with the *in vitro* observation that permeability of BMS-911543 across caco-2 monolayers was high. BMS-911543 has a permeability coefficient (5×10^{-5} cm/s) comparable to the values for compounds that exhibit good absorption in humans. **Supplementary Figure S3B** demonstrates that F_a is sensitive to the changes in solubility, indicative of solubility-limited absorption. Thus, enhancement in solubility (e.g., by formulation) could improve the absorption of BMS-911543 if a higher dose is required for BMS-911543 development.

In the initial model, the V_{ss} was estimated to be $\geq$2 L/kg (140 L for a subject with 70 kg body weight) based on the tissue-to-plasma partitioning coefficients predicted by the compound's physicochemical properties.[9] The estimate for the V_{ss} value obtained from population PK analysis of the clinical data was $\sim$25 L when F was assumed to be 0.5 (clinically observed V_{ss}/F:$\sim$50 L). The discrepancy between the V_{ss} predicted by the initial PBPK model and the clinical observation suggested that more detailed understanding of tissue distribution would improve the modeling efforts. For this reason, a rat tissue distribution study was conducted to help fill knowledge gaps regarding distribution. There are several assumptions when making the V_{ss} prediction using the rat tissue distribution data. First, the distribution of BMS-911543 in human tissues is similar to the distribution in rat tissues. Second, the tissue-to-plasma ratio of total radioactivity is a close estimate for the value of unchanged BMS-911543. Third, experimental data obtained from rat tissues after single dosing represent the tissue-to-plasma partition coefficients at steady state. By replacing the *in silico* calculated tissue-to-plasma partition coefficients with the observed data in rats, the estimate of V_{ss} was decreased to 0.26 L/kg (18.2 L for a subject with 70 kg body weight), which was generally in line with the values observed in humans.

The metabolic clearance was characterized by the enzyme kinetics in cDNA-expressed CYP enzymes (**Figure 1**). Because the model incorporating the kinetic parameters from the expressed CYP enzyme systems gave an overprediction of the plasma concentrations compared to the clinical observation, we proposed that such discrepancy of the *in vitro-in vivo* extrapolation was due to an underestimation of the metabolic clearance of BMS-911543. To eliminate the possibility that BMS-911543 is metabolized by other unknown metabolic pathways, the human plasma samples were analyzed to look for unknown metabolites (**Supplementary Figure S2**). The results from human plasma profiling work revealed three additional secondary metabolites (M2, M3, and M4; **Supplementary Figure S1**). M2, M3, and M4 were partially or completely characterized and all judged to be downstream metabolites formed from M1. In the absence of other unknown metabolic pathways, a metabolic scaling factor of 4 was incorporated into the enzyme kinetics of the known pathways to compensate for the underestimation of the metabolic clearance. The decision to apply the scaling factor of 4 to the parameter of K_m was based on the fitting performance to the day 1 concentration-time profiles observed in the FIH study (alternatively, one could change V_{max}). We acknowledge that many factors could hamper the estimation of metabolic clearance and confound the *in vitro-in vivo* extrapolation.[10] The metabolism pathways of BMS-911543 used for elimination in humans can only be completely established by human ADME study with radiolabeled BMS-911543.[11] A reevaluation of the clearance of BMS-911543 followed by refinement of the PBPK model will be necessary when human ADME results for BMS-911543 become available.

CYP1A2 TDI inactivation parameters were not determined before the FIH study and not incorporated into the initial model. However, saturation of metabolism alone did not explain the magnitude of PK nonlinearity observed after multiple dosing. In search of the additional underlying mechanism, sensitivity analysis was conducted to explore

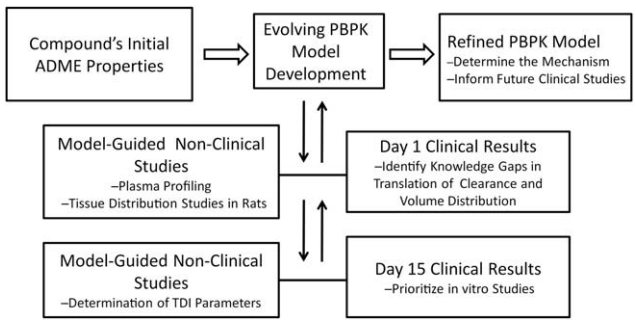

Figure 7 Physiologically based pharmacokinetic (PBPK) model-guided bi directional translation of the compound's absorption, distribution, metabolism, and excretion (ADME) information to determine the mechanism of time-dependent and dose-dependent nonlinear pharmacokinetics after compound's early clinical studies. Arrows denote the continuing bidirectional translation of ADME information.

the impact of the TDI inactivation parameters (K_I, k_{inact}) on AUC at various doses. Both CYP1A2 TDI inactivation parameters produced a significant impact on the AUC of BMS-911543 with changes of dose (**Supplementary Figure S4**). The results of sensitivity analysis suggested that CYP1A2 TDI might be the key factor leading to the greater than dose-proportional exposure after multiple dosing of BMS-911543. Investigation of the TDI by determination of kinetic parameters (K_I and k_{inact}) in human liver microsomes confirmed the TDI of CYP1A2 at clinically relevant concentrations (**Figure 2**). However, quantitative translation of the *in vitro* kinetic parameters to model the *in vivo* effect proved to be challenging. Based on the fitting performance to the clinical concentration-time profiles, the K_I value was allowed to vary from the experimental value of 2.9 ± 0.9 μM. The best fit was obtained with a K_I value of 11 ± 3.4 μM. Prediction of TDI in human studies using parameters generated from *in vitro* experiments continues to be a major challenge for all CYP enzymes.[12] As well, it has been well recognized that there are significant differences in values of inactivation parameters generated among laboratories.[13] This is analogous to the issue of interlaboratory differences for permeability values using caco-2 cell monolayers.[14] This has led to the adoption of a "best practice" recommendation to correct interlaboratory variation in caco-2 permeability values that includes conducting analysis against dual calibrators, such as verapamil and metoprolol. A calibration algorithm has not been developed to correct for such differences in TDI inactivation parameters. In addition, the rate constant of the enzyme degradation (k_{deg}) also significantly impacts the magnitude of TDI-mediated inactivation. For simplicity, the default value for k_{deg} was used in our prediction.

The validity of the model is supported by the good prediction of the complicated PKs observed in the clinical study described in this article, which included both single and multiple dosing regimens ranging from 5 to 240 mg across 9 dose levels. However, the model should continue evolving once new clinical data become available. In particular, the input values for both K_m and K_I parameters are modified from experimental data by fitting the model to clinical observation, and, thus, they are not identifiable. Additional studies, for instance, human ADME and drug-drug interaction studies would provide additional constraining power to enable more accurate estimation of their true values.

PBPK modeling has become a powerful tool that provides mechanistic understanding of a compound's PK behavior and when properly constructed can be very useful in predicting changes in behavior in various clinical settings.[15] However, there are many challenges in constructing a PBPK model to adequately describe the human PKs for a compound during the early phase of clinical development. Initial PBPK models, based on ADME data obtained either from *in vitro* systems or from animal species, often fail to describe clinical observations in FIH studies. Reasons for the model failure can be the insufficient information describing the ADME processes available during early development or the inadequate translatability of the available ADME data from preclinical to clinical. However, discrepancies in predicted behavior vs. observed behavior revealed by the initial model often contain valuable information. The discrepancies revealed may indicate the presence of knowledge gaps stemming from incomplete information or may challenge the validity of calculated or measured parameters and lead to additional nonclinical experimentation to fill the gaps. This is a model-guided reverse translation process that can also help determine which nonclinical study should be conducted with high priority. The initial model can then evolve with the addition of the newly generated drug-related properties. This refinement cycle can continue through additional iterations once new clinical data become available. Eventually, the optimized PBPK model can be used to achieve satisfactory forward translatability for future clinical PK predictions. **Figure 7** illustrates the bidirectional translation of BMS-911543's ADME information based on PBPK modeling.

In conclusion, the results presented here indicate that the bidirectional PBPK model-based translation of ADME information is a useful strategy in general practice for mechanistic understanding of a compound's disposition during early clinical development. Integration of a plausible PBPK model into early clinical development was possible even for a compound with complex ADME properties like BMS-911543 (namely, low solubility and TDI and induction of an enzyme while being a substrate for the same enzyme) that exhibits dose-dependent and time-dependent nonlinear pharmacokinetics, but will likely require researchers to use a forward and back translation paradigm between experimental data and model.

Acknowledgment. The authors thank Dr Iain Gardner (SimCYP, Sheffield, UK) for helpful discussions.

Conflict of Interest. The authors were all employees of Bristol-Myers Squibb at the time of conducting the research described in the article.

Author Contributions. L.Z., J.G., H.Y., and J.L. designed research. X.G. and J.L. performed research. L.Z., J.G., H.Y., X.G., and J.L. contributed new reagents or analytical tools. L.Z., J.G., H.Y., and J.L. analyzed data. L.Z., J.G., H.Y., J.L., E.M., and W.G.H. wrote the manuscript.

1. Di, L. *et al.* A perspective on the prediction of drug pharmacokinetics and disposition in drug research and development. *Drug Metab. Dispos.* **41**, 1975–1993 (2013).
2. Shardlow, C.E., Generaux, G.T., Patel, A.H., Tai, G., Tran, T. & Bloomer, J.C. Impact of physiologically based pharmacokinetic modeling and simulation in drug development. *Drug Metab. Dispos.* **41**, 1994–2003 (2013).
3. Jones, H. & Rowland-Yeo, K. Basic concepts in physiologically based pharmacokinetic modeling in drug discovery and development. *CPT Pharmacometrics Syst. Pharmacol.* **2**, e63 (2013).
4. Zhao, P., Rowland, M. & Huang, S.M. Best practice in the use of physiologically based pharmacokinetic modeling and simulation to address clinical pharmacology regulatory questions. *Clin. Pharmacol. Ther.* **92**, 17–20 (2012).
5. Varma, M.V., Lai Y., Feng, B., Litchfield, J., Goosen, T.C. & Bergman, A. Physiological based modeling of pravastatin transporter-mediated hepatobiliary disposition and drug-drug interactions. *Pharm. Res.* **29**, 2860–2873 (2012).
6. Purandare, A.V. *et al.* Characterization of BMS-911543, a functionally selective small-molecule inhibitor of JAK2. *Leukemia* **26**, 280–288 (2012).
7. Artursson, P. & Karlsson, J. Correlation between oral drug absorption in humans and apparent drug permeability coefficients in human intestinal epithelial (Coca-2) cells. *Biochem. Biophys. Res. Commun.* **175**, 880–885 (1991).
8. Pardanani, A. *et al.* BMS-911543, a selective JAK2 inhibitor: a multicenter phase 1/2a study in myelofibrosis. *Blood.* **122**, abstract 664 (2013).
9. Poulin, P. & Theil, F.P. Prediction of pharmacokinetics prior to in vivo studies. 1. Mechanism-based prediction of volume of distribution. *J. Pharm. Sci.* **91**, 129–156 (2002).
10. Obach, R.S. Prediction of human clearance of twenty-nine drugs from hepatic microsomal intrinsic clearance data: an examination of in vitro half-life approach and nonspecific binding to microsomes. *Drug Metab. Dispos.* **27**, 1350–1359 (1999).
11. Zhou, L. *et al.* Disposition of [1'-(14)C]stavudine after oral administration to humans. *Drug Metab. Dispos.* **38**, 655–666 (2010).
12. Grimm, S.W. *et al.* The conduct of in vitro studies to address time-dependent inhibition of drug-metabolizing enzymes: a perspective of the pharmaceutical research and manufacturers of America. *Drug Metab. Dispos.* **37**, 1355–1370 (2009).
13. Rowland Yeo, K., Walsky, R.L., Jamei, M., Rostami-Hodjegan, A. & Tucker, G.T. Prediction of time-dependent CYP3A4 drug-drug interactions by physiologically based pharmacokinetic modeling: impact of inactivation parameters and enzyme turnover. *Eur. J. Pharm. Sci.* **43**, 160–173 (2011).
14. Bentz, J. *et al.* Variability in P-glycoprotein inhibitory potency (IC_{50}) using various in vitro experimental systems: implications for universal digoxin drug-drug interaction risk assessment decision criteria. *Drug Metab. Dispos.* **41**, 1347–1366 (2013).
15. Zhao, P. *et al.* Applications of physiologically based pharmacokinetic (PBPK) modeling and simulation during regulatory review. *Clin. Pharmacol. Ther.* **89**, 259–267 (2011).

Supplementary information accompanies this paper on the *CPT: Pharmacometrics & Systems Pharmacology* website (http://www.wileyonlinelibrary.com/psp4)